Check for updates

Highly efficient benzyl alcohol valorisation *via* the *in situ* synthesis of H_2O_2 and associated reactive oxygen species†

Gregory Sharp,‡[a] Richard J. Lewis, [ID] *‡[a] G. Magri,[b] J. Liu,[c] David J. Morgan, [ID] [a,d] Thomas E. Davies,[a] Ángeles López-Martín,[a] Damien M. Murphy, [ID] [b] Andrea Folli, [ID] [e] Liwei Chen,[c] Xi Liu*[c,f] and Graham J. Hutchings [ID] *[a]

The selective oxidation of chemical feedstocks *via in situ* production of reactive oxygen species (H_2O_2, $^{\bullet}OOH$, $^{\bullet}OH$, $^{\bullet}O_2^-$), represents an attractive, environmentally friendly alternative to the use of stoichiometric oxidants. Within this contribution, we demonstrate the efficacy of the *in situ* approach to the selective oxidation of benzyl alcohol to the commodity chemical benzaldehyde, with the alloying of Au with Pd shown to be key in significantly promoting catalytic performance. The immobilisation of AuPd nanoalloys, particularly on to a γ-Al_2O_3 carrier, is demonstrated to result in high selective utilisation of H_2 (*ca.* 80%), overcoming a major hurdle that has often precluded the adoption of the *in situ* approach to chemical synthesis on a commercial scale, while also achieving yields of benzaldehyde in excess of 60%, over successive experiments, representing a significant step towards competitiveness with traditional oxidative processes reliant on stoichiometric oxidants. Evaluation of catalyst performance towards individual reaction pathways (*i.e.* H_2O_2 direct synthesis and benzyl alcohol oxidation in the presence of preformed H_2O_2), analysis by EPR spectroscopy and radical quenching experiments, indicates that reactive oxygen-based species (ROS), rather than H_2O_2, are primarily responsible for the observed catalysis. While the origin of these oxygen-based radicals is not fully understood, we consider that they are generated primarily as reaction intermediates formed during H_2O_2 synthesis over active metal surfaces.

Green foundation

1. Currently the oxidative valorisation of alcohols is reliant on costly and atom-inefficient stoichiometric oxidants, which generate large quantities of unwanted by-products. However, the *in situ* production of hydrogen peroxide and related oxidative species avoids these concerns and allows for significant process intensification.

2. To date, low yields and poor H_2 utilisation have prevented the adoption of an *in situ* approach to feedstock upgrading. This work demonstrates that through rational catalyst design it is possible to overcome these drawbacks, with our optimised AuPd catalyst offering H_2 selectivity approaching 80%, and product yields in excess of 60% through successive reactions.

3. Further catalyst design is required in order to improve reactivity and H_2 utilisation rates.

[a]*Max Planck-Cardiff Centre on the Fundamentals of Heterogeneous Catalysis FUNCAT, Cardiff Catalysis Institute, School of Chemistry, Cardiff University, Translational Research Hub, Maindy Road, Cardiff, CF24 4HQ, UK. E-mail: LewisR27@Cardiff.ac.uk, Hutch@Cardiff.ac.uk*
[b]*School of Chemistry, Cardiff University, Main Building, Park Place, Cardiff, CF10 3AT, UK*
[c]*In situ Centre for Physical Sciences, School of Chemistry and Chemical, Frontiers Science Centre for Transformative Molecules, Shanghai 200240, P. R. China. E-mail: LiuXi@stju.edu.cn*

[d]*HarwellXPS, Research Complex at Harwell (RCaH), Didcot, OX11 0FA, UK*
[e]*Net Zero Innovation Institute, Cardiff Catalysis Institute, School of Chemistry, Cardiff University, Translational Research Hub, Maindy Road, Cardiff, CF24 4HF, UK*
[f]*School of Chemistry and Chemical Engineering, Ningxia University, Yinchuan 750021, P. R. China*
†Electronic supplementary information (ESI) available. See DOI: https://doi.org/10.1039/d5gc00680e
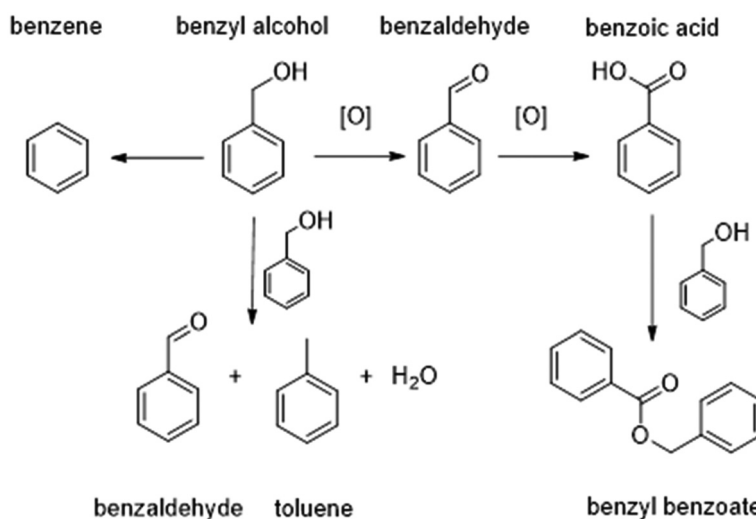‡These authors contributed equally to this work.

Introduction

Primary alcohol valorisation to the corresponding aldehyde is of significant industrial importance, representing key feedstocks in sectors ranging from perfumery to dyestuff and agrochemicals.[1] Typically, the selective oxidation of these platform chemicals on an industrial scale is reliant on the utilisation of energy- and atom-inefficient stoichiometric oxidants, resulting in the production of undesirable and complex product streams.[2] Such concerns have led to an interest in alternative, aerobic approaches, with numerous reports demonstrating that is possible to achieve high aldehyde yields when using molecular oxygen.[3] However, while the green credentials associated with aerobic oxidation are clear, such routes typically require elevated reaction temperatures to be effective.[3–6] Thus, while the use of O_2 as the terminal oxidant can overcome the atom-inefficiency concerns of current industrial routes, reliant on stoichiometric oxidants, the utilisation of aerobic routes may still be hampered by poor energy usage. Alternatively, unlike O_2-mediated pathways, the utilisation of preformed H_2O_2 allows for relatively low reaction temperatures to be exploited,[7–10] but suffers from (i) high production costs of the oxidant, (ii) the continual dilution of product streams (iii) the presence of proprietary stabilising agents, which can lead to reactor corrosion, and (iv) the need for constant monitoring to avoid the development of H_2O_2 hot spots.

Offering the potential for improved atom efficiency compared to the use of alternative stoichiometric oxidants (and preformed H_2O_2) and lower operating temperatures than aerobic pathways, the *in situ* synthesis and subsequent utilisation of H_2O_2 and related reactive oxygen species (ROS; $^\bullet OOH$, $^\bullet OH$, $^\bullet O_2^-$), in chemical feedstock valorisation is an area of significant and growing research interest.[11–13] However, while considerable efforts have been made in this field, particularly around propylene epoxidation,[14–16] very few examples of an *in situ* approach to oxidative upgrading which rival the per-

formance metrics of mature industrial processes have been reported. In many cases, a combination of poor selective H_2 utilisation, rapid catalyst deactivation, and the formation of complex product streams, necessitating energy-intensive purification steps, have prevented development beyond the laboratory scale. Indeed, the presence of H_2, necessary for H_2O_2 and ROS production, in conjunction with effective hydrogenation catalysts, such as Pd and Pt, which are typically used for H_2O_2 synthesis,[17–22] are responsible for many of these challenges.[23–25]

The *in situ* selective oxidation of benzyl alcohol to benzaldehyde (Scheme 1), is one such chemical transformation that has received considerable research interest.[26–28] In part, this is due to the limited number of reaction products and the relatively well-known pathways to their formation. However, benzaldehyde is a valuable feedstock in its own right, finding use in the cosmetics and pharmaceutical sectors. Indeed, the benzaldehyde market was valued at approximately $580 million per annum in 2024,[29] so interest in the oxidative upgrading of this feedstock chemical is not purely academic.

Supported AuPd nanoalloys have been reported to offer exceptional activity towards the aerobic valorisation of several platform chemicals[30,31] and are also considered among the state-of-the-art for the direct synthesis of H_2O_2.[32] With regard to the latter transformation, the alloying of Pd with Au has been demonstrated to significantly enhance catalytic performance (compared to the monometallic analogues), due to a combination of electronic and isolation effects, resulting in improved activity and selectivity towards H_2O_2.[33–36] In part, this has been attributed to the weaker interaction between the metal surface and the synthesised H_2O_2, when compared to Pd-only surfaces.[37] Importantly, the formation of these mixed metal surfaces has recently been shown to favour the release of highly reactive oxygen species, which are formed as intermediates during H_2O_2 synthesis.[38] The potential for such ROS to be utilised in chemical synthesis, particularly in processes where

Scheme 1 General reaction scheme for the oxidation of benzyl alcohol.

proton-abstraction is key, is particularly intriguing and in this contribution, we investigate the performance of supported AuPd nanoparticles to effectively generate H_2O_2 (and related ROS), and the subsequent efficacy of these species towards the *in situ* selective oxidation of benzyl alcohol to benzaldehyde.

Experimental

Catalyst synthesis

Mono- and bi-metallic 1%Au–Pd/X catalysts were prepared (on a weight basis) by a wet co-impregnation of chloride metal precursors onto a range of common oxide supports (TiO_2 (P25), γ-Al_2O_3, CeO_2, Nb_2O_5, ZrO_2), based on a methodology previously reported in the literature.[39] The procedure to produce 0.5% Au–0.5%Pd/Al_2O_3 (2 g) is outlined below, with a similar methodology being utilised for all catalysts.

Aqueous $PdCl_2$ solution (1.667 mL, [Pd] = 6 mg mL^{-1}, Merck) and aqueous $HAuCl_4 \cdot 3H_2O$ solution (0.8263 mL, [Au] = 12.25 mg mL^{-1}, Strem Chemicals) were mixed in a 50 mL round-bottom flask and heated to 65 °C with stirring (1000 rpm) in a thermostatically controlled oil bath, with the total volume fixed to 16 mL using H_2O (HPLC grade, Fisher Scientific). When a temperature of 65 °C was reached, γ-Al_2O_3 (1.98 g, Fischer Scientific) was added over the course of 5 min with constant stirring. The resulting slurry was stirred at 65 °C for a further 15 min, after which the temperature was raised to 95 °C for 16 h to allow for the complete evaporation of water. The resulting solid was mechanically ground prior to heat treatment under a reductive atmosphere (flowing 5% H_2/Ar, 500 °C, 4 h, and ramp rate of 10 °C min^{-1}).

Catalyst testing

Note 1: The reaction conditions used within this study operate below the flammability limits of gaseous mixtures of H_2 and O_2.

Note 2: The conditions used within this work for H_2O_2 synthesis and degradation have previously been investigated, where the presence of CO_2 as a diluent for reactant gases and methanol as a co-solvent has been identified as key to maintaining high catalytic efficacy towards H_2O_2 production.[40] In particular, the CO_2 gaseous diluent has been found to act as an *in situ* promoter of H_2O_2 stability through dissolution in the reaction solution and the formation of carbonic acid. We have previously reported that the use of the CO_2 diluent has a comparable promotive effect to that observed when acidifying the reaction solution to a pH of 4 using HNO_3.[41]

Direct synthesis of H_2O_2

Hydrogen peroxide synthesis activity was evaluated using a Parr Instruments stainless steel autoclave with a nominal volume of 50 mL and a maximum working pressure of 2000 psi, equipped with a PTFE liner. To test each catalyst for H_2O_2 synthesis, the autoclave liner was charged with catalyst (0.01 g), solvent (5.6 g methanol, HPLC grade, Fisher Scientific) and H_2O (2.9 g, HPLC grade, Fisher Scientific). The charged autoclave was then purged three times with 5% H_2/CO_2 (100 psi) before filling with 5%H_2/CO_2 to a pressure of 420 psi, followed by the addition of 25%O_2/CO_2 (160 psi). The pressures of 5%H_2/CO_2 and 25%O_2/CO_2 were taken as gauge pressures. The reaction mixture was stirred (1200 rpm) for 0.5 h, with the temperature being maintained at 20 °C. Reactor temperature control was achieved using a HAAKE K50 bath/circulator using an appropriate coolant. The reactor was not continuously supplied with gas. H_2O_2 productivity was determined by titrating aliquots of the final solution after reaction with acidified $Ce(SO_4)_2$ (0.01 M) in the presence of ferroin indicator. Catalyst productivities are reported as $mol_{H_2O_2}$ kg_{cat}^{-1} h^{-1}.

In all cases, reactions were run multiple times, over multiple batches of catalyst, with the data presented an average of these experiments. Catalytic activity towards H_2O_2 synthesis was found to be consistent to within ±2% based on multiple reactions.

Degradation of H_2O_2

Catalytic activity towards H_2O_2 degradation (*via* hydrogenation and decomposition pathways) was determined in a manner similar to that used for measuring the H_2O_2 direct synthesis activity of a catalyst. The autoclave liner was charged with methanol (5.6 g, HPLC grade, Fisher Scientific), H_2O_2 (50 wt% 0.69 g, Merck), H_2O (2.21 g, HPLC grade, Fisher Scientific) and catalyst (0.01 g), with the solvent composition equivalent to a 4 wt% H_2O_2 solution. From the solution, two aliquots of 0.05 g were removed and titrated with acidified $Ce(SO_4)_2$ solution using ferroin as an indicator to determine an accurate concentration of H_2O_2 at the start of the reaction. The charged autoclave was then purged three times with 5%H_2/CO_2 (100 psi) before filling with 5%H_2/CO_2 (420 psi). The pressures of 5% H_2/CO_2 was taken as gauge pressure. The reaction mixture was stirred (1200 rpm) for 0.5 h, with the reaction temperature maintained at 20 °C. After the reaction was complete, the catalyst was removed from the reaction solvents *via* filtration and as described previously, two aliquots of 0.05 g were titrated against the acidified $Ce(SO_4)_2$ solution using ferroin as an indicator. Catalyst degradation activity is reported as $mol_{H_2O_2}$ kg_{cat}^{-1} h^{-1}.

In all cases, reactions were run multiple times, over multiple batches of catalyst, with the data presented an average of these experiments. Catalytic activity towards H_2O_2 degradation was found to be consistent to within ±5% based on multiple reactions.

Benzyl alcohol oxidation *via in situ* production of H_2O_2

Note 3: Reaction conditions utilised within this study are based on those previously identified by our laboratory for the *in situ* oxidation of benzyl alcohol, they have been maintained in this work to allow for ease of comparison to the established literature.

The oxidation of benzyl alcohol has been investigated in a 50 mL Parr Instruments stainless steel autoclave, equipped with PTFE liner. The autoclave liner was charged with catalyst (0.01 g), methanol (7.13 g, HPLC grade, Fisher Scientific) and

benzyl alcohol (1.04 g, 9.62 mmol, Merck) along with 0.5 mL of the internal standard mesitylene (0.43 g, 3.58 mmol, Merck). The charged autoclave was then purged three times with 5% H_2/CO_2 (100 psi) before filling with 5% H_2/CO_2 to a pressure of 420 psi, followed by the addition of 25%O_2/CO_2 (160 psi). The pressures of 5%H_2/CO_2 and 25%O_2/CO_2 were taken as gauge pressures. The reactor was subsequently heated to 50 °C, followed by stirring at 1200 rpm for 0.5 h, unless otherwise stated. The reactor was not continuously supplied with gas. After the reaction was complete, the reactor was cooled in ice water to a temperature of 15 °C, after which a gas sample was taken for analysis by gas chromatography using a Varian CP-3380 equipped with a TCD detector and a Porapak Q column, to allow for the determination of H_2 conversion. Once cooled to the desired temperature, the catalyst was removed from the reaction solvents *via* filtration and the liquid product yield was determined by gas chromatography using a Varian 3200 GC, equipped with a CP Wax 42 column and FID. The concentration of residual H_2O_2 was determined by titrating aliquots of the final solution after reaction with acidified $Ce(SO_4)_2$ (0.01 M) in the presence of ferroin indicator.

Further studies were conducted in the presence of radical quenching agents (Na_2SO_3 or $NaNO_2$) at a concentration of 0.05 M.

The total capacity of the autoclave was determined *via* water displacement to allow for accurate determination of H_2 conversion and H_2 selectivity. When equipped with the PTFE liner and liquid reagents the total available gaseous space within the autoclave and is equivalent to 2.8 mmol of H_2.

In all cases, reactions were run multiple times, over multiple batches of catalyst, with the data presented an average of these experiments. For benzyl alcohol oxidation total product yield was observed to be consistent to within ±4% based on multiple reactions.

H_2 conversion (eqn (1)), benzyl alcohol conversion (eqn (2)), product yield (eqn (3)), product selectivity (eqn (4)) and H_2 selectivity (eqn (5)) are defined as follows:

$$H_2 \text{ conversion } (\%) = \frac{mmol_{H_2(t(0))} - mmol_{H_2(t(1))}}{mmol_{H_2(t(0))}} \times 100 \quad (1)$$

$$\begin{aligned}&\text{Benzyl alcohol conversion } (\%)\\&= \frac{\text{benzyl alcohol reacted (mmol)}}{\text{benzyl alcohol initial (mmol)}} \times 100\end{aligned} \quad (2)$$

$$\text{Product yield } (\%) = \frac{\text{product (mmol)}}{\text{benzyl alcohol initial (mmol)}} \times 100 \quad (3)$$

$$\text{Product selectivity } (\%) = \frac{\text{product } (mmol)}{\text{benzyl alcohol converted } (mmol)} \times 100 \quad (4)$$

$$H_2 \text{ selectivity} = \frac{\text{benzaldehyde (mmol)}}{H_2 \text{ conversion (mmol)}} \times 100 \quad (5)$$

Catalyst re-useability in benzyl alcohol oxidation *via in situ* production of H_2O_2

In order to determine catalyst reusability, a similar procedure to that outlined above for benzyl alcohol oxidation *via* the *in situ* production of H_2O_2 was followed utilizing 0.3 g of catalyst. Following the initial test, the catalyst was recovered by filtration, washed with MeOH (5 g, HPLC grade, Fischer Scientific) and dried (30 °C, 16 h, under vacuum). Next, 0.01 g of material from the recovered catalyst sample was used to conduct a standard oxidation experiment.

Gas replacement experiments for the oxidation of benzyl alcohol *via* the *in situ* production of H_2O_2

An identical procedure to that outlined above for the oxidation of benzyl alcohol was followed for a reaction time of 0.5 h. After this, stirring was stopped and the reactant gas mixture was vented prior to replacement with the standard pressures of 5%H_2/CO_2 (420 psi) and 25% O_2/CO_2 (160 psi). The reaction mixture was then stirred (1200 rpm) for a further 0.5 h. To collect a series of data points, as in the case of Fig. 4, it should be noted that individual experiments were carried out and the reactant mixture was not sampled online.

Benzyl alcohol upgrading using individual gaseous reagents (H_2 or O_2) or commercial H_2O_2

An identical procedure to that outlined above for the *in situ* oxidation of benzyl alcohol was followed for a reaction time of 0.5 h, with the reactor charged with either 5%H_2/CO_2 (420 psi) or 25% O_2/CO_2 (160 psi), with total reactor pressure maintained at 580 psi with CO_2. As above, the reactor was not continually supplied with gas. Additional experiments were conducted using commercial H_2O_2 (50 wt%, Merck), at a concentration equal to that which may be synthesised during the *in situ* oxidation of benzyl alcohol, assuming total H_2 conversion to H_2O_2. In this case, the preformed H_2O_2 was added to the reactor prior to the reaction commencing (*i.e.* not continually introduced) and total pressure was maintained at 580 psi using CO_2.

Radical trapping experiments with electron paramagnetic resonance spectroscopy

The catalyst (0.01 g), methanol (7.13 g, HPLC grade, Fisher Scientific) and benzyl alcohol (1.04 g, 9.6 mmol, Merck) were added to the reactor along with 0.5 mL of the internal standard mesitylene (0.43 g, 3.58 mmol, Merck) and 5,5-dimethyl-1-pyrroline *N*-oxide (12 µL, Merck). The reactor was purged three times with 5%H_2/CO_2 (100 psi) and then filled with 5% H_2/CO_2 (420 psi) and 25%O_2/CO_2 (160 psi). The reactor was then heated to 50 °C and once the temperature was reached, stirring (1200 rpm) was commenced for 0.5 h. Once the reaction was complete, the reactor was purged with 20 bar N_2 for 20 min before the catalyst was separated by filtration and the filtered solution loaded into a 1.1 mm quartz tube for analysis by EPR spectroscopy.

Various blank reactions were also analysed by EPR spectroscopy to determine any background activity.

Continuous wave X-band EPR spectra were recorded at 298 K using a Bruker EMX Micro spectrometer equipped with a Bruker ER 4123d dielectric resonator. Spectra were recorded at *ca.* 9.75 GHz and 2 mW microwave power, with 100 kHz field modulation frequency, 1 G field modulation amplitude, 5×10^4 receiver gain, 10.00 ms conversion time and 5.02 ms time constant. EPR spectra were simulated using the EasySpin toolbox[42] running within the MathWorks Matlab environment.

Catalyst characterisation

A Kratos Axis Ultra DLD spectrometer was used to collect X-ray photoelectron spectra utilising a monochromatic Al K_α X-ray source operating at 144 W (12 mA × 12 kV). Samples for analysis were mounted by pressing into double-sided adhesive tape attached to a microscope slide attached to a standard Kratos sample bar assembly. Data was collected using the Hybrid mode with a Slot aperture, yielding an analysis area of *ca.* 700 × 300 μm². The pass energies for acquisition were 40 (step size 0.1 eV) and 160 eV (step size 1 eV) for high-resolution and survey spectra, respectively. Sample charging effects were minimised through magnetically confined low-energy electrons using the Kratos immersion lens system and the resulting spectra were calibrated to the C(1s) line at 284.8 eV for all samples, a secondary charge reference of the Al(2p) peak was also used to confirm the suitability of the C(1s) line and found to be 74.5 eV, typical for Al_2O_3. The uncertainty in binding energies is ±0.2 eV. All data was processed using CasaXPS v2.3.27. The data was analysed typically using a Shirley background, although a linear background was used where the signal was low or negative. Peak areas were corrected using modified Wagner sensitivity factors. Peak fitting where required was achieved using line shape models derived from bulk compounds (Pd and Au metal foils and PdO) using Voigt-like functions.

Brunauer Emmett Teller (BET) surface area measurements were conducted using a Quadrasorb surface area analyser. A 5-point isotherm of each material was measured using N_2 as the adsorbate gas. Samples were degassed at 250 °C for 2 h prior to the surface area being determined by 5-point N_2 adsorption at −196 °C, and data analysed using the BET method. Surface area measurements of key samples (and corresponding bare supports) are reported in Table S1,† with a minor loss in surface area found to result from metal deposition and thermal treatment of the catalytic samples.

The bulk structure of the catalysts was determined by powder X-ray diffraction using a (θ–θ) PANalytical X'pert Pro powder diffractometer using a Cu K_α radiation source, operating at 40 keV and 40 mA. Standard analysis was carried out using a backfilled sample, between 2θ values of 10–80°. Phase identification was carried out using the International Centre for Diffraction Data (ICDD). XRD analysis of supported AuPd catalysts prepared on a range of common oxide supports is reported in Figure S1A–E,† with no clear reflections associated with either precious metal, which may be attributed to the low total metal loading.

Total metal loading of key catalytic samples was quantified by digestion of as-prepared (dried only) samples *via* micro-wave-assisted aqua regia digestion. Digested samples were analysed *via* inductively coupled plasma mass spectrometry (ICP-MS). All calibrants were matrix-matched and measured against a five-point calibration using certified reference materials purchased from PerkinElmer and certified internal standards acquired from Agilent. Actual metal loadings of key catalytic samples are provided in Table S2A and B.†

Total metal leaching from the supported catalyst was quantified *via* inductively coupled plasma mass spectrometry (ICP-MS). Post-reaction solutions were analysed using an Agilent 7900 ICP-MS equipped with I-AS auto-sampler. All samples were diluted by a factor of 10 using HPLC grade H_2O (1%HNO_3 and 0.5% HCl matrix). All calibrants were matrix-matched and measured against a five-point calibration using certified reference materials purchased from PerkinElmer and certified internal standards acquired from Agilent.

DRIFTS measurements were taken on a Bruker Tensor 27 spectrometer fitted with a mercury cadmium telluride (MCT) detector. A sample was loaded into the Praying Mantis high temperature (HVC-DRP-4) *in situ* cell before exposure to N_2 and then 1% CO/N_2 at a flow rate of 50 cm³ min⁻¹. A background spectrum was obtained using KBr, and measurements were recorded every 1 min at room temperature. Once the CO adsorption bands in the DRIFT spectra ceased to increase in size, the gas feed was changed back to N_2 and measurements were repeated until no change in subsequent spectra was observed.

Aberration-corrected scanning transmission electron microscopy (AC-STEM) was performed using a probe-corrected S/TEM instrument (Thermo Fisher, Thermis Z), operating at 300 kV. The latter instrument was equipped with a Super-X EDS detector for high-spatial XEDS characterization.

Results and discussion

Our initial studies identified the crucial role of the support in dictating catalytic activity towards the direct synthesis and subsequent degradation of H_2O_2 (Table 1). In keeping with earlier investigations[43,44] into the performance of AuPd catalysts prepared by a co-impregnation procedure, a strong correlation between reactivity and the choice of nanoparticle carrier was observed, with the high activity of the 0.5%Au–0.5%Pd/TiO_2 (75 mol$_{H_2O_2}$ kg$_{cat}$⁻¹ h⁻¹), and 0.5%Au–0.5%Pd/Al_2O_3 (62 mol$_{H_2O_2}$ kg$_{cat}$⁻¹ h⁻¹), catalysts towards H_2O_2 direct synthesis, in comparison to alternative oxide supported analogues, clear. Numerous studies have identified the role of catalyst support in dictating both reactivity and selectivity in the direct synthesis of H_2O_2, through the control of alloy formation and particle dispersion, amongst other factors. Indeed, we have recently demonstrated the role of the particle carrier in dictating metal speciation, particularly that of Pd, a key factor in the production of the oxidant, and direct the reader to these earlier works for an in-depth analysis of many of the formulations reported in Table 1.[44]

The performance of the TiO_2(P25) and γ-Al_2O_3-based formulations is particularly noteworthy given the relatively challen-

Table 1 Catalytic activity of AuPd catalysts towards the direct synthesis and the subsequent degradation of H_2O_2, as a function of the catalyst support

Catalyst	Productivity/$mol_{H_2O_2}$ kg_{cat}^{-1} h^{-1}	H_2O_2 Conc./wt%	H_2 Conv./%	H_2O_2 Sel./%	Degradation/$mol_{H_2O_2}$ kg_{cat}^{-1} h^{-1}
0.5%Au–0.5%Pd/TiO_2	75	0.15	38	36	390
0.5%Au–0.5%Pd /Al_2O_3	62	0.12	33	34	366
0.5%Au–0.5%Pd /CeO_2	30	0.06	14	40	289
0.5%Au–0.5%Pd /Nb_2O_5	25	0.06	11	43	255
0.5%Au–0.5%Pd /ZrO_2	30	0.04	12	47	270

H_2O_2 direct synthesis reaction conditions: mass of catalyst (0.01 g), H_2O (2.9 g), MeOH (5.6 g), 5%H_2/CO_2 (420 psi), 25%O_2/CO_2 (160 psi), 0.5 h, 20 °C, 1200 rpm. H_2O_2 degradation reaction conditions: catalyst (0.01 g), H_2O_2 (50 wt% 0.68 g) H_2O (2.22 g), MeOH (5.6 g), 5%H_2/CO_2 (420 psi), 0.5 h, 20 °C, 1200 rpm.

ging reaction temperatures utilised within this work and the poor stability of H_2O_2 under such conditions, with sub-ambient temperatures widely applied to inhibit competitive H_2O formation via H_2O_2 hydrogenation and decomposition pathways.[40]

Subsequent investigation of catalytic performance towards the *in situ* oxidation of benzyl alcohol (Fig. 1, with additional data reported in Table S3†) revealed no clear correlation between individual reaction pathways (*i.e.* H_2O_2 synthesis and benzyl alcohol valorisation), with almost all formulations offering similar reactivity (<3.0% product yield, 100% benzaldehyde selectivity), despite the relatively varied activity towards H_2O_2 synthesis (Table 1). The limited reactivity of the 0.5%Au–0.5%Pd/TiO_2 catalyst towards the *in situ* oxidation of benzyl alcohol is particularly noteworthy given the high H_2O_2 synthesis activity observed over this formulation. While it is important to highlight the variation in reaction conditions used to probe individual reaction pathways, such observations, particularly when considered alongside recent studies[38] which

report the ability of Au to promote the desorption of oxygen-based radical species (˙OOH, ˙OH, ˙O_2^-) from AuPd surfaces, may indicate that H_2O_2 is not the primary species responsible for the observed catalysis. Indeed, we have recently proposed the key role of such radical species for the selective oxidation of alternative chemical feedstocks.[45,46]

The 0.5%Au–0.5%Pd/Al_2O_3 catalyst was found to offer exceptional activity towards benzyl alcohol oxidation (22.7% product yield, 98% benzaldehyde selectivity). Indeed, the performance of this formulation is particularly noteworthy given the high selective utilisation of H_2 in the valorisation of benzyl alcohol (76%), with poor H_2 efficiency a longstanding hurdle for numerous *in situ* approaches to feedstock valorisation. In particular, catalytic hydrogenation of both reagents and products, as well as the degradation of H_2O_2 to H_2O via hydrogenation pathways, have been identified as major contributors to process inefficiency.[23] Although here we highlight our recent contributions centred around the *in situ* ammoximation of cyclic ketones to the corresponding oxime, which has demonstrated that such concerns may be overcome through rational catalyst and process design.[47]

Together with other laboratories, we have previously identified a strong dependence between the catalytic performance of bimetallic AuPd formulations towards the direct synthesis of H_2O_2,[35,40,48,49] as well as the aerobic valorisation of a range of chemical feedstocks (including benzyl alcohol), and the elemental composition of active sites.[50–53] In keeping with these earlier studies, and with a focus on γ-Al_2O_3 supported formulations, we subsequently established the synergistic enhancement that results from the formation of AuPd nanoalloys (Table 2 and Fig. 2, with additional data reported in Table S4†). This enhancement can, at least in part be attributed to the electronic modification of Pd species through alloying with Au, as evidenced by CO-DRIFTS (Figure S2 and ESI Note 1†), and XPS analysis (Figure S3†), with further investigation of the catalytic series by TEM (Table 3, with representative micrographs reported in Figure S4†), ruling out variation in mean particle size, another key parameter known to dictate catalytic activity, especially to H_2O_2 synthesis,[54] as a source for the underlying promotive effect observed upon the formation of AuPd alloys.

Again, we highlight the discrepancy in catalytic activity towards H_2O_2 direct synthesis and the oxidative valorisation of
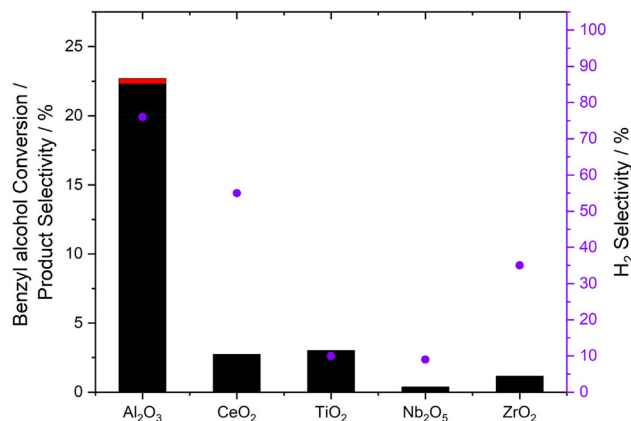

Fig. 1 Catalytic activity of bimetallic 0.5%Au–0.5%Pd/Al_2O_3 catalysts towards the selective oxidation of benzyl alcohol via *in situ* H_2O_2 synthesis, as a function of the catalyst support. *Key*: benzaldehyde (*black bars*), benzoic acid (*red bars*); H_2 selectivity towards benzaldehyde (*purple circles*). Reaction conditions: mass of catalyst (0.01 g), benzyl alcohol (1.04 g, 9.62 mmol), MeOH (7.1 g), 5%H_2/CO_2 (420 psi), 25%O_2/CO_2 (160 psi), 50 °C, 0.5 h, 1200 rpm. Note: H_2 selectivity was determined, based on the mol of H_2 utilised in the formation of benzaldehyde.

Table 2 Activity of bimetallic 1%AuPd/Al$_2$O$_3$ catalysts towards the direct synthesis and subsequent degradation of H$_2$O$_2$

Catalyst	Productivity/mol$_{H_2O_2}$ kg$_{cat}^{-1}$ h^{-1}	H$_2$O$_2$ Conc./wt%	H$_2$ Conv./%	H$_2$O$_2$ Sel./%	Degradation/mol$_{H_2O_2}$ kg$_{cat}^{-1}$ h^{-1}
1%Au/Al$_2$O$_3$	2	0.001	B.D.L	—	22
0.75%Au–0.25%Pd/Al$_2$O$_3$	70	0.14	21	59	287
0.5%Au–0.5%Pd/Al$_2$O$_3$	62	0.12	33	34	366
0.25%Au–0.75%Pd/Al$_2$O$_3$	59	0.12	32	34	289
1%Pd/Al$_2$O$_3$	43	0.09	26	30	200
0.5%Pd/Al$_2$O$_3$	32	0.07	17	34	119

H$_2$O$_2$ direct synthesis reaction conditions: Mass of catalyst (0.01 g), H$_2$O (2.9 g), MeOH (5.6 g), 5%H$_2$/CO$_2$ (420 psi), 25%O$_2$/CO$_2$ (160 psi), 0.5 h, 20 °C, 1200 rpm. H$_2$O$_2$ degradation reaction conditions: mass of catalyst (0.01 g), H$_2$O$_2$ (50 wt% 0.68 g) H$_2$O (2.22 g), MeOH (5.6 g), 5%H$_2$/CO$_2$ (420 psi), 0.5 h, 20 °C, 1200 rpm. B.D.L: below the detection limit.

Table 3 Effect of Au : Pd ratio on mean nanoparticle size of 1%AuPd/Al$_2$O$_3$ catalysts

Catalyst	Mean particle size/ nm (S.D)	Reaction rate/ mmol$_{aldehyde}$ mmol$_{metal}^{-1}$ h^{-1}
1%Au/Al$_2$O$_3$	28.9 (26.1)	0
0.75%Au–0.25%Pd/Al$_2$O$_3$	2.4 (1.4)	2.06 × 10^3
0.5%Au–0.5%Pd/Al$_2$O$_3$	3.5 (2.2)	5.92 × 10^3
0.25%Au–0.75%Pd/Al$_2$O$_3$	3.1 (1.8)	5.82 × 10^3
1%Pd/Al$_2$O$_3$	5.1 (4.8)	3.4 × 10^3

Catalysts exposed to a reductive heat treatment (5%H$_2$/Ar, 500 °C, 4 h, 10 °C min^{-1}). Reaction rate is based on theoretical metal loading, at a reaction time of 0.5 h.

Fig. 2 Catalytic activity of bimetallic 1%AuPd/Al$_2$O$_3$ catalysts towards the selective oxidation of benzyl alcohol *via in situ* H$_2$O$_2$ synthesis, as a function of Au : Pd ratio. *Key*: benzaldehyde (*black bars*), benzoic acid (*red bars*), H$_2$ selectivity (*purple circles*). Reaction conditions: mass of catalyst (0.01 g), benzyl alcohol (1.04 g, 9.62 mmol), MeOH (7.1 g), 5% H$_2$/CO$_2$ (420 psi), 25%O$_2$/CO$_2$ (160 psi), 50 °C, 0.5 h, 1200 rpm. Note: H$_2$ selectivity is determined based on the mol of H$_2$ utilised in the formation of benzaldehyde. The 1%Au/Al$_2$O$_3$ offered no measurable activity towards benzyl alcohol oxidation.

benzyl alcohol over this series of catalyst formulations, which we consider further implicates the contribution of alternative oxidative agents in the observed catalysis. Indeed, the 0.25% Au–0.75%Pd/Al$_2$O$_3$ formulation can be seen to offer a significantly improved performance towards benzyl alcohol oxidation compared to the 0.5%Au–0.5%Pd/Al$_2$O$_3$ analogue, while also offering high H$_2$ efficiency (81%), despite the similar rates of H$_2$O$_2$ synthesis observed over both formulations, which may indicate the potential secondary role of H$_2$O$_2$ in benzyl alcohol oxidation.

With the clear enhancement in catalytic activity identified upon the introduction of Au into supported Pd catalysts, we were motivated to further investigate a subset of these formulations (*i.e.* the 1%Pd/Al$_2$O$_3$ and 0.5%Pd–0.5%Au/Al$_2$O$_3$ catalysts), in order to broaden our understanding of the underlying cause for the observed trends in catalytic performance.

Further evaluation focussing on these key catalysts established the negligible contribution of purely oxidative (using a 25%O$_2$/CO$_2$ atmosphere) (0.2–0.8% product yield) or reductive (using a 5%H$_2$/CO$_2$ atmosphere) (0.4–1.0% product yield), pathways towards benzyl alcohol conversion (Figure S5†). These observations, particularly the low product yields detected under an aerobic atmosphere, may be unsurprising given the reaction temperatures within this study (50 °C), with temperatures exceeding 80 °C typically required for aerobic benzyl alcohol oxidation over AuPd surfaces.[55,56] When utilising a H$_2$-only gaseous atmosphere, relatively low concentrations of benzaldehyde were detected (approx. 0.1% yield), which can be attributed to the incomplete purging of dissolved oxygen from the reaction medium and the resulting pro-
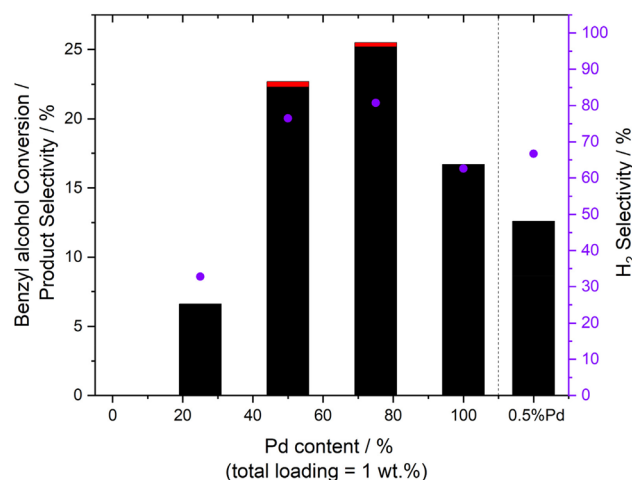
duction of low concentrations of H$_2$O$_2$ and related radical species. Notably, in the absence of exogenous O$_2$, toluene was also observed and indeed was found to be the major product (0.3–0.8% yield), which can be related to the known reactivity of Pd-based catalysts towards disproportionation pathways.[1,57] Subsequent studies also indicated that a significant improvement in benzyl alcohol conversion may be obtained *via in situ* H$_2$O$_2$ production, compared to that observed when using the preformed oxidant at a concentration identical to that which would be obtained if all the H$_2$ present in the *in situ* system was selectively converted to H$_2$O$_2$. This is likely a result of the complete addition of the *ex situ* generated H$_2$O$_2$ at the start of the reaction, although the effect of the proprietary stabilising agents present in commercially available H$_2$O$_2$ on catalytic performance should also be considered. Additionally, such observations again further highlight the potential for reactive oxygen species, rather than H$_2$O$_2$ itself, to be primarily respon-

sible for the observed catalysis. Regardless, given the relatively high costs associated with commercial H_2O_2, the comparative economic and environmental benefits of the *in situ* approach are clear and we consider these will only strengthen with the application of non-fossil derived H_2 sources.

Extended reaction time studies comparing the catalytic efficacy of key formulations are reported in Fig. 3 (additional data are presented in Table S5A and B,† with determination of catalyst stability, through ICP-MS analysis of post-reaction solutions, at key time points reported in Table S6†). As over our standard reaction time (0.5 h), the higher catalytic activity of the 0.5%Au–0.5%Pd/Al_2O_3 catalyst was clear (27.1% product yield, 97% benzaldehyde selectivity), significantly outperforming the 1%Pd/Al_2O_3 analogue (19.0% product yield, 100% benzaldehyde selectivity), over 1.5 h of reaction. The high

benzaldehyde selectivity offered by both formulations indicates the suppression of competitive reaction pathways, and can primarily be related to the presence of unconverted substrate, with earlier works focussed on aerobic oxidation of benzyl alcohol, revealing that the presence of benzyl alcohol (at concentrations as low as 2%), in addition to a range of other alcohols (although notably not methanol, the solvent used in this study), can inhibit the overoxidation of benzaldehyde to the corresponding acid.[58]

Notably, catalytic performance was found to plateau after relatively short reaction times (45 minutes), with minimal additional conversion of benzyl alcohol observed beyond this
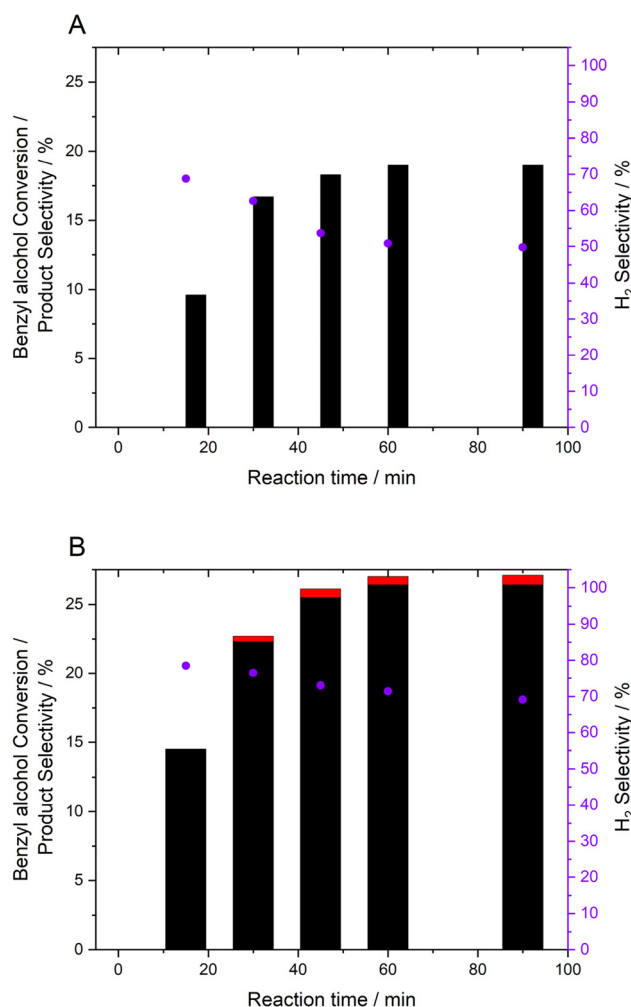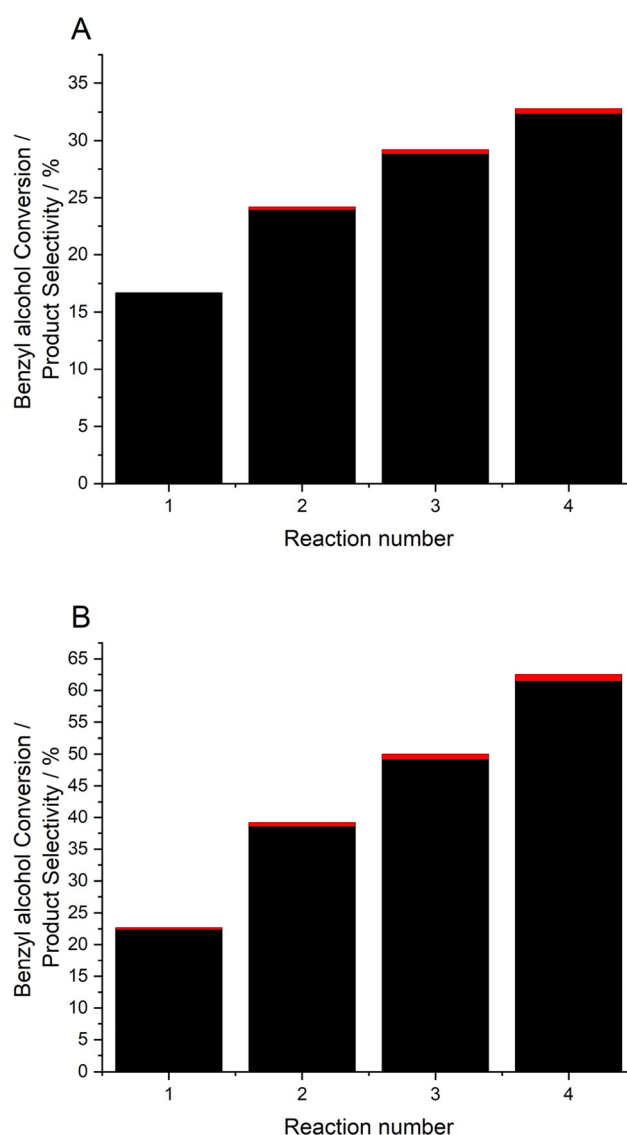

Fig. 3 Comparison of catalytic performance towards the selective oxidation of benzyl alcohol *via in situ* H_2O_2 synthesis over the (A) 1%Pd/Al_2O_3 and (B) 0.5%Au−0.5%Pd/Al_2O_3 catalysts, as a function of reaction time. *Key*: benzaldehyde (*black bars*), benzoic acid (*red bars*), H_2 selectivity (*purple circles*). Reaction conditions: mass of catalyst (0.01 g), benzyl alcohol (1.04 g, 9.62 mmol), MeOH (7.1 g), 5%H_2/CO_2 (420 psi), 25%O_2/CO_2 (160 psi), 50 °C, 1200 rpm. Note: H_2 selectivity is determined based on the mol of H_2 utilised in the formation of benzaldehyde.

Fig. 4 Comparison of catalytic performance towards the selective oxidation of benzyl alcohol *via in situ* H_2O_2 synthesis, over the (A) 1%Pd/Al_2O_3 and (B) 0.5%Au−0.5%Pd/Al_2O_3 catalysts, over successive reactions. *Key*: benzaldehyde (*black bars*), benzoic acid (*red bars*), H_2 selectivity (*purple circles*). Reaction conditions: mass of catalyst (0.01 g), benzyl alcohol (1.04 g, 9.62 mmol), MeOH (7.1 g), 5%H_2/CO_2 (420 psi), 25%O_2/CO_2 (160 psi), 50 °C, 0.5 h, 1200 rpm.

time point. While this may be indicative of catalyst deactivation, it is important to highlight the relatively high rates of H_2 conversion (approx. 80%) and the potential for the reaction to become limited by H_2 availability, particularly given the excess of benzyl alcohol (in comparison to H_2) present in the system. Interestingly, the 1%Pd/Al$_2$O$_3$ and 0.5%Au–0.5%Pd/Al$_2$O$_3$ catalysts displayed similar H_2 conversion rates over the course of the reaction (Table S5A and B†), with this metric reaching approximately 90% over 1.5 h. However, as with our standard reaction time, the bimetallic formulation offered significantly improved selectivity based on H_2 compared to the Pd-only analogue (69 and 50% H_2 selectivity for the 0.5%Au–0.5%Pd/Al$_2$O$_3$ and 1%Pd/Al$_2$O$_3$ catalysts respectively). Again we consider the improved efficiency of the AuPd formulation noteworthy given the concerns associated with selective H_2 utilisation during the valorisation of chemical feedstocks *via in situ* H_2O_2 production.[13,23]

Given the plateau in catalytic performance and the high rates of H_2 conversion observed for the AuPd and Pd-only formulations during our time-on-line study and the potential for the reaction to become limited by H_2 availability, we next investigated catalytic performance over sequential *in situ* benzyl alcohol experiments, where gaseous reagents were replaced at 0.5 h intervals (Fig. 4, with additional information reported in Table S7†). For both catalysts, the yield of benzaldehyde increased considerably over four successive reactions, although it should be noted that this increase was not linear, which may suggest some loss in catalyst performance or restructuring of catalytic sites with time. However, the influence of reagent availability, particularly in the case of the AuPd catalyst should also be considered given the relatively high rates of benzyl alcohol conversion observed upon sequential reactions (>40% over two successive reactions). Regardless, the reactivity of the 0.5%Au–0.5%Pd/Al$_2$O$_3$ catalyst is note-
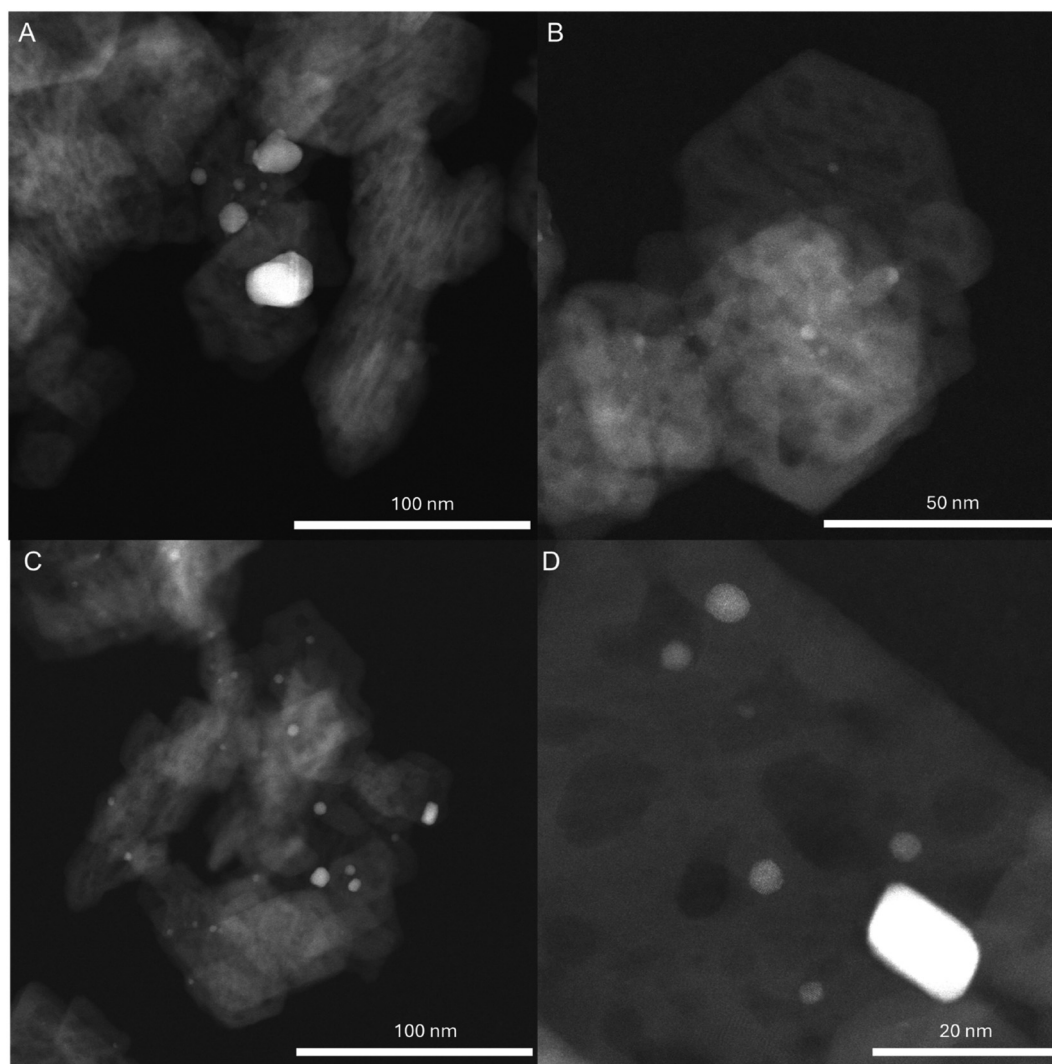

Fig. 5 Representative HAADF-STEM of the as-prepared (A and B) 1%Pd/Al$_2$O$_3$ and (C and D) 0.5%Au−0.5%Pd/Al$_2$O$_3$ catalysts, demonstrating the bimodal distribution in particle size.

worthy achieving a product yield of 62% (98% benzaldehyde selectivity) over four successive reactions, significantly outperforming the 1%Pd/Al$_2$O$_3$ analogue (33% product yield, 100% benzaldehyde selectivity) as well as previous reports in the literature (Table S8†), highlighting the potential improvements in the *in situ* approach to alcohol valorisation that may be achieved through rational catalyst design. Further comparison to aerobic approaches benzyl alcohol oxidation over AuPd surfaces are reported in Table S9,† and indicate the competitiveness of the *in situ* approach, although it is clear that further technical evaluation is required (life cycle analysis, process safety techno-economic analysis) to fully understand the technical feasibility of the *in situ* approach.

Catalyst stability was subsequently evaluated through re-use experiments (Figure S6†). While a loss in catalytic activity was observed over both formulations, the high selectivity towards benzaldehyde and in the case of the AuPd catalyst, selectivity towards H$_2$ observed upon initial use was largely retained. Interestingly, the AuPd formulation was also found to retain a greater proportion of its initial activity over three uses (approx. 80%) compared to the Pd-only analogue (50%). In part, this can be attributed to the increased stability of the bimetallic catalyst, as evidenced by ICP-MS analysis of post-reaction solutions, where the presence of Au was found to considerably inhibit Pd leaching (Table S10†), which aligns well with previous studies into AuPd-based formulations,[47] although it is likely that other factors beyond metal loss are responsible for the variation in performance upon reuse.

Evaluation of the as-prepared catalytic materials *via* STEM-HAADF (Fig. 5) imaging revealed a relatively broad particle size distribution, which is typical of the wet impregnation route to catalyst synthesis, particularly for bimetallic AuPd-based formulations. However, here we highlight that for both formulations mean particle size was found to be between approximately 3 and 5 nm (Table 3 and Figure S4†). Notably, unlike in our earlier studies which have focussed on Pd-based catalysts prepared by a similar wet impregnation technique, the monometallic catalyst also displays a bimodal particle size distribution, which may evidence the role of nanoparticle carrier in dictating particle size, with these previous works primarily focussed on the use of TiO$_2$ as the catalyst support.[27] Subsequent STEM-XEDS mapping of individual nanoparticles within the bimetallic formulation (Fig. 6, with additional data reported in Fig. S7 and S8†), confirmed the presence of AuPd random alloys, regardless of particle size, although the larger particles (>10 nm) were found to be Au-rich, again in keeping with earlier works into analogous formulations.[33]

The alloying of Au with Pd has been well-reported to improve catalytic selectivity towards H$_2$O$_2$ through the inhibition of competitive degradation pathways that lead to the formation of H$_2$O (*i.e.* O–O bond dissociation), as well as promoting desorption of the synthesised H$_2$O$_2$.[37] Recently, the ability of AuPd surfaces to also promote the desorption of reaction intermediates (*i.e.* ˙O$_2^-$, ˙OH and ˙OOH) formed during H$_2$O$_2$ synthesis has also been described,[38] with further works demonstrating the efficacy of these highly reactive oxygen-
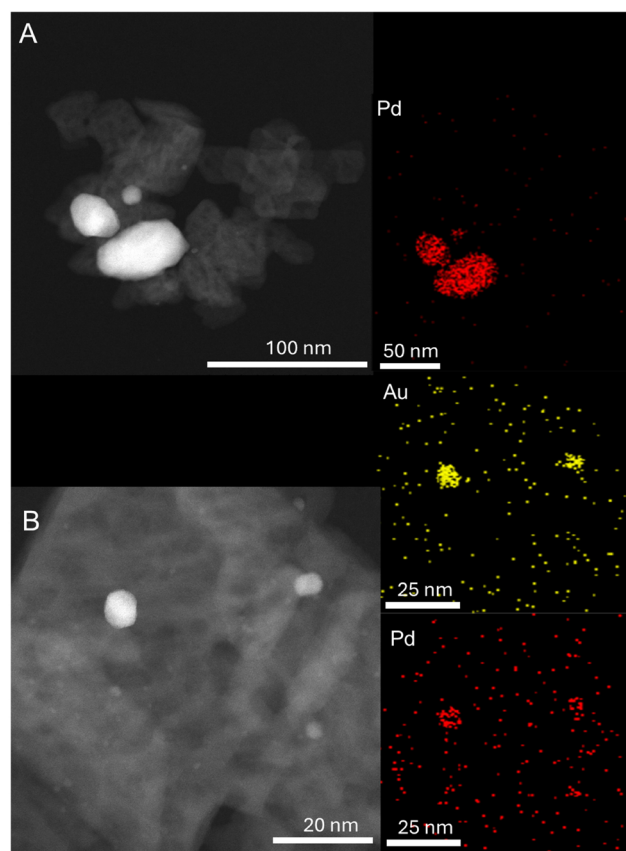

Fig. 6 HAADF-STEM and corresponding X-EDS analysis of the as-prepared (A) 1%Pd/Al$_2$O$_3$ and (B) 0.5%Au−0.5%Pd/Al$_2$O$_3$ catalysts.

based species to catalyze both selective oxidation[59] and total degradation of chemical feedstocks.[60] With these earlier works in mind, we subsequently conducted a series of spin-trapping electron paramagnetic resonance (EPR) spectroscopy measurements using 5,5-dimethyl-1-pyrroline *N*-oxide (DMPO) as the radical trapping agent.

Fig. 7A reports the EPR spectra obtained under *in situ* benzyl alcohol oxidation reaction conditions, with control experiments conducted in the presence of a H$_2$O-only solvent reported in Fig. 7B (additional blank reactions in Fig. S9†). Over both catalyst formulations, a clear signal attributed to an O-centred methoxy radical (CH$_3$O˙) trapped by DMPO, forming a DMPO-OCH$_3$ aminoxyl radical adduct (with g_{iso} = 2.006, $a_{iso}(^{14}$N$)$ = 1.559 mT and $a_{iso}(^1$H$_\beta)$ = 2.260 mT), when a methanol solvent was utilised. The presence of such methoxy species is considered to result from the ability of methanol to act as a scavenger for oxygen-based radicals generated during H$_2$O$_2$ synthesis or *via* catalytic degradation of the synthesised H$_2$O$_2$.[61,62]

To confirm the presence of a reactive oxygen progenitor species further studies were conducted, utilising a H$_2$O-only solvent (Fig. 7B). For both catalysts, experiments conducted in the absence of benzyl alcohol (spectra i and ii), the spectra were dominated by a signal symptomatic of trapped oxygen-based radicals (g_{iso} = 2.006, $a_{iso}(^{14}$N$)$ = 1.493 mT, and $a_{iso}(^1$H$_\beta)$
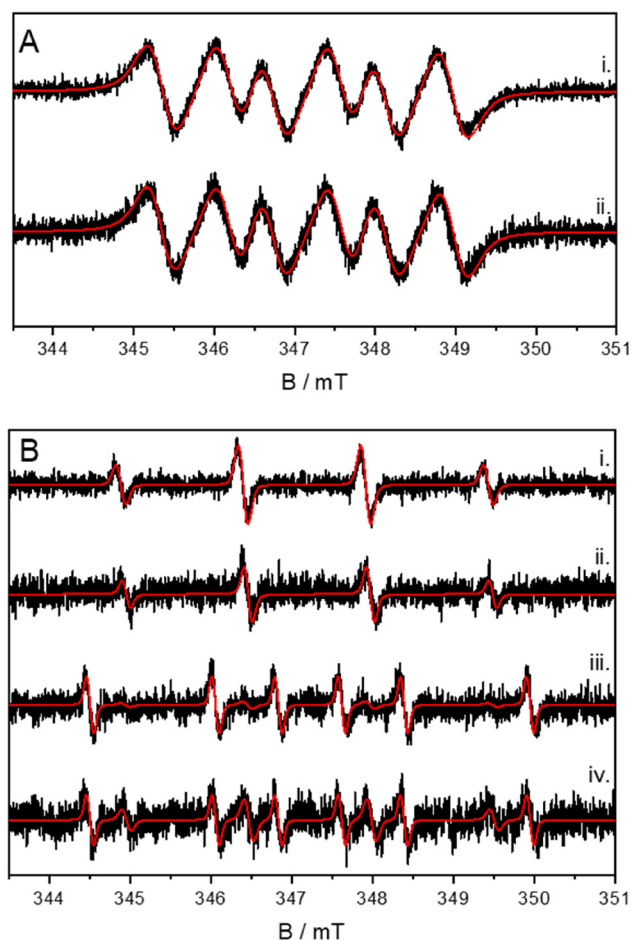
Fig. 7 Experimental (black) and simulated (red) EPR spectra of DMPO-radical adducts formed during the *in situ* oxidation of benzyl alcohol. (A) Reactions conducted in methanol at 50 °C, with benzyl alcohol (9.62 mmol), 5% H_2/CO_2 (420 psi), and 25% O_2/CO_2 (160 psi) in the presence of DMPO and the (i) 1%Pd/Al_2O_3 or (ii) 0.5%Au−0.5%Pd/Al_2O_3 catalysts. (B) Control reactions conducted in water at 50 °C, in the presence of DMPO and (i) 1%Pd/Al_2O_3 or (ii) 0.5%Au−0.5%Pd/Al_2O_3 under *in situ* conditions and the absence of benzyl alcohol, with analogous experiments over the (iii) 1%Pd/Al_2O_3 and (iv) 0.5%Au−0.5%Pd/Al_2O_3 catalysts under *in situ* conditions and in the presence of benzyl alcohol.

= 1.493 mT). However, we were unable to distinguish between trapped hydroxyl ($^{\bullet}$OH) and hydroperoxyl ($^{\bullet}$OOH) species due to the short half-life of the DMPO-OOH adduct (1–4 min), which rapidly decays to DMPO-OH in the presence of unreacted DMPO. Unsurprisingly, in the absence of the gaseous reagents (Fig. 7B spectra iii and iv) the signal associated with the DMPO-OH adduct decreased significantly, and the spectra was dominated by a new signal consistent with a DMPO-trapped C-centred species (PhCH$^{\bullet}$(OH))[63] (characterised by $g_{iso} = 2.006$, $a_{iso}(^{14}N) = 1.559$ mT, and $a_{iso}(^{1}H_\beta) = 2.260$ mT), suggesting that PhCH$^{\bullet}$(OH) is the first intermediate in the oxidation of benzyl alcohol. Control experiments (Figure S6†) in the absence of the catalyst revealed no signal from either trapped O- or C-centred radical species, indicating that the generation of such reactive species is a catalytic process, with

additional experiments further identifying the presence of the DMPO-OCH$_3$ nitroxide radical.

To support our EPR studies, we subsequently investigated the effect of radical quenching agents (Na_2SO_3 and $NaNO_2$ separately and at a concentration of 0.05 M), on catalytic performance towards *in situ* benzyl alcohol oxidation (Table S11†). A substantial decrease in benzyl alcohol conversion was observed, further indicating the role of radical species in the reaction mechanism. Notably, when taken together with our EPR investigations, these experiments indicate that the oxygen-centred radicals are the primary species responsible for the observed catalysis. The non-innocent nature of the methanol solvent is also indicated. However, the role of the solvent-based radicals is unclear, that is we were unable to determine if the methanol simply acts as a radical propagating agent or if there is also involvement in the reaction mechanism, possibly through the promotion of H-abstraction from the alcohol moiety, which is considered key in the formation of the aldehyde.[64,65] Furthermore, we recognise the direct role of the solvent in the synthesis of H_2O_2 and associated ROS, as outlined by Flaherty and co-workers;[66] as such, there is clearly a need to develop a detailed understanding of solvent involvement in the reaction mechanism.

Conclusions and future perspectives

The *in situ* synthesis and efficient utilisation of H_2O_2 (and associated reactive oxygen species), over AuPd nanoalloys has been demonstrated to offer high efficacy in the selective oxidation of benzyl alcohol to the corresponding aldehyde, offering improved performance compared to the use of preformed H_2O_2 or aerobic oxidative pathways. In particular, the role of the support was found to be crucial in dictating catalytic performance towards benzyl alcohol valorisation, with the γ-Al_2O_3 supported formulation outperforming analogous catalysts prepared on a range of other common oxides by a factor of 10, despite the increased activity of alternative formulations towards H_2O_2 direct synthesis. Such observations suggest that H_2O_2 itself is not the primary species responsible for the observed catalysis, with further detailed analysis by electron paramagnetic spectroscopy indicating the role of both reactive oxygen species (*e.g.* $^{\bullet}$OOH, $^{\bullet}$OH, and $^{\bullet}O_2^-$ generated as intermediates during H_2O_2 synthesis, *via* H_2O_2 decomposition or a combination of both processes) and methoxy-based ($^{\bullet}$CH$_3$O) radicals (resulting from the radical scavenging ability of the methanol solvent) within the reaction mechanism. Although the extent to which these methoxy-based species contribute directly to the observed catalysis is not fully understood, one can hypothesise that they contribute to the initial proton-abstraction from the alcohol moiety (PhCH$_2$O*H*) or may act as a propagating agent for subsequent ROS formation. However, with the known ability of the solvent to play a crucial role in the formation of H_2O_2 (and associated ROS), as well as in the inhibition of benzaldehyde overoxidation, there is clear potential for the solvent to be involved in numerous mechanistic

steps, which must be fully understood if this approach to chemical synthesis is to be fully developed.

The alloying of Pd with Au was found to considerably enhance the selective utilisation of H_2, overcoming a key hurdle which has limited the adoption of the *in situ* approach for the oxidative valorisation of many chemical feedstocks and the resulting $AuPd/Al_2O_3$ catalyst was found to significantly outperform previous examples reported in the literature, achieving yields of benzaldehyde in excess of 60%, with near total selectivity. However, there is still scope for further improvements in catalytic design in order to improve H_2 utilisation rates and catalyst stability.

Our observation of relatively large concentrations of residual H_2O_2 within benzyl alcohol oxidation product streams and the demonstration that H_2O_2 itself it not the primary oxidative species in benzyl alcohol valorisation also indicates that there is scope for further improvement in catalyst design, to shift selectivity away from H_2O_2 and towards ROS formation. However, there is a need to ensure effective utilisation of the radical flux and minimise competitive termination reactions, which lead to the unselective utilisation of H_2.

There are now a growing number of reports which outline the potential benefits of the *in situ* approach to chemical synthesis, particularly for oxime manufacture and the valorisation of methane. Indeed, such chemistry may find particular application in the production of low-value/high-volume commodity chemicals, such as adipic acid, cyclohexanone, cyclohexanol and phenol, as well as other benzyl alcohol derivatives, where the high cost of pre-formed H_2O_2, relative to that of the desired product, has prevented progression to industrial production, despite promising results at the laboratory scale. However, it is clear that in many cases, concerns around catalytic selectivity and deactivation, often resulting from the presence of H_2, required to generate the oxidant *in situ*, must be addressed.

While the potential of the *in situ* technology is particularly exciting, it is important to note that several hurdles must first be overcome if it is to rival industrially operated processes. From a safety perspective, it is imperative that explosive mixtures of H_2/O_2 are avoided. Additionally, as with industrial processes that currently utilise preformed H_2O_2 (*e.g.* cyclohexanone ammoximation and propylene oxide manufacture), there is a need to ensure hot-spots of H_2O_2 are avoided, both from a safety aspect and process efficiency standpoint. There is clearly also a need to further enhance catalyst stability to ensure lifetimes required for industrial application are met.

Author contributions

G.S and R.J.L conducted catalyst synthesis, testing, and corresponding data analysis. G.S., R.J.L, J.L, G.M., D.J.M., T.E.D., A.L, and X.L. conducted catalyst characterisation and corresponding data processing. R.J.L., D.M.M, A.F., L.C. and X.L provided technical advice. R.J.L and G.J.H contributed to the design of the study and results interpretation. R.J.L wrote the manuscript and ESI,† with all authors commenting on and amending both documents. All authors discussed and contributed to this work.

Data availability

The data supporting this article have been included as part of the ESI.†

Conflicts of interest

The authors declare no conflict of interest.

Acknowledgements

References

1 C. E. Chan-Thaw, A. Savara and A. Villa, *Catalysts*, 2018, **8**, 431.

2 B. L. Ryland and S. S. Stahl, *Angew. Chem., Int. Ed.*, 2014, **53**, 8824–8838.

3 P. Wu, Y. Cao, L. Zhao, Y. Wang, Z. He, W. Xing, P. Bai, S. Mintova and Z. Yan, *J. Catal.*, 2019, **375**, 32–43.

4 W. Zhou, G. Chen, B. Yu, J. Zhou, J. Qian, M. He and Q. Chen, *Appl. Catal., A*, 2020, **592**, 117417.

5 H. Göksu, H. Burhan, S. D. Mustafov and F. Şen, *Sci. Rep.*, 2020, **10**, 5439.

6 A. Savara, I. Rossetti, C. E. Chan-Thaw, L. Prati and A. Villa, *ChemCatChem*, 2016, **8**, 2482–2491.

7 W. Hou, N. A. Dehm and R. W. J. Scott, *J. Catal.*, 2008, **253**, 22–27.

8 K. Kawamura, T. Yasuda, T. Hatanaka, K. Hamahiga, N. Matsuda, M. Ueshima and K. Nakai, *Chem. Eng. J.*, 2016, **285**, 49–56.

9 C. Xu, L. Zhang, Y. An, X. Wang, G. Xu, Y. Chen and L. Dai, *Appl. Catal., A*, 2018, **558**, 26–33.

10 A. L. Cánepa, V. R. Elías, V. M. Vaschetti, E. V. Sabre, G. A. Eimer and S. G. Casuscelli, *Appl. Catal., A*, 2017, **545**, 72–78.

11 N. O'Callaghan and J. A. Sullivan, *Appl. Catal., B*, 2014, **146**, 258–266.

12 B. Puértolas, A. K. Hill, T. García, B. Solsona and L. Torrente-Murciano, *Catal. Today*, 2015, **248**, 115–127.

13 R. J. Lewis and G. J. Hutchings, *Acc. Chem. Res.*, 2024, **57**, 106–119.

14 T. Hayashi, K. Tanaka and M. Haruta, *J. Catal.*, 1998, **178**, 566–575.

15 J. Huang, E. Lima, T. Akita, A. Guzmán, C. Qi, T. Takei and M. Haruta, *J. Catal.*, 2011, **278**, 8–15.

16 S. Kanungo, D. M. Perez Ferrandez, F. Neira D'Angelo, J. C. Schouten and T. A. Nijhuis, *J. Catal.*, 2016, **338**, 284–294.

17 S. Quon, D. Y. Jo, G.-H. Han, S. S. Han, M.-G. Seo and K. Lee, *J. Catal.*, 2018, **368**, 237–247.

18 Q. Liu, J. C. Bauer, R. E. Schaak and J. H. Lunsford, *Appl. Catal., A*, 2008, **339**, 130–136.

19 S. Yu, X. Cheng, Y. Wang, B. Xiao, Y. Xing, J. Ren, Y. Lu, H. Li, C. Zhuang and G. Chen, *Nat. Commun.*, 2022, **13**, 4737.

20 L. F. D. L. e Freitas, B. Puértolas, J. Zhang, B. Wang, A. S. Hoffman, S. R. Bare, J. Pérez-Ramírez, J. W. Medlin and E. Nikolla, *ACS Catal.*, 2020, **10**, 5202–5207.

21 F. Wang, C. Xia, S. P. de Visser and Y. Wang, *J. Am. Chem. Soc.*, 2019, **141**, 901–910.

22 D. W. Flaherty, *ACS Catal.*, 2018, **8**, 1520–1527.

23 G. Wang, W. Du, X. Duan, Y. Cao, Z. Zhang, J. Xu, W. Chen, G. Qian, W. Yuan, X. Zhou and D. Chen, *Chem. Catal.*, 2021, **1**, 885–895.

24 Q. Chen and E. J. Beckman, *Green Chem.*, 2008, **10**, 934–938.

25 S.-Y. Ye, S. Hamakawa, S. Tanaka, K. Sato, M. Esashi and F. Mizukami, *Chem. Eng. J.*, 2009, **155**, 829–837.

26 J. Lyu, L. Niu, F. Shen, J. Wei, Y. Xiang, Z. Yu, G. Zhang, C. Ding, Y. Huang and X. Li, *ACS Omega*, 2020, **5**, 16865–16874.

27 C. M. Crombie, R. J. Lewis, R. L. Taylor, D. J. Morgan, T. E. Davies, A. Folli, D. M. Murphy, J. K. Edwards, J. Qi, H. Jiang, C. J. Kiely, X. Liu, M. S. Skjøth-Rasmussen and G. J. Hutchings, *ACS Catal.*, 2021, **11**, 2701–2714.

28 M. Santonastaso, S. J. Freakley, P. J. Miedziak, G. L. Brett, J. K. Edwards and G. J. Hutchings, *Org. Process Res. Dev.*, 2014, **18**, 1455–1460.

29 Benzaldehyde Market – Growth, Industry Applications & Market Trends, *via* **https://www.futuremarketinsights.com/reports/benzaldehyde-market**, accessed 07.02.2025.

30 L. Kesavan, R. Tiruvalam, M. H. A. Rahim, M. I. bin Saiman, D. I. Enache, R. L. Jenkins, N. Dimitratos, J. A. Lopez-Sanchez, S. H. Taylor, D. W. Knight, C. J. Kiely and G. J. Hutchings, *Science*, 2011, **331**, 195–199.

31 C. M. Crombie, R. J. Lewis, D. Kovačič, D. J. Morgan, T. E. Davies, J. K. Edwards, M. S. Skjøth-Rasmussen and G. J. Hutchings, *Catal. Lett.*, 2021, **151**, 164–171.

32 J. K. Edwards, B. Solsona, E. N. Ntainjua, A. F. Carley, A. A. Herzing, C. J. Kiely and G. J. Hutchings, *Science*, 2009, **323**, 1037.

33 D. Kovačič, R. J. Lewis, C. M. Crombie, D. J. Morgan, T. E. Davies, Á. López-Martín, T. Qin, C. S. Allen, J. K. Edwards, L. Chen, M. S. Skjøth-Rasmussen, X. Liu and G. J. Hutchings, *Green Chem.*, 2023, **25**, 10436–10446.

34 T. Ricciardulli, S. Gorthy, J. S. Adams, C. Thompson, A. M. Karim, M. Neurock and D. W. Flaherty, *J. Am. Chem. Soc.*, 2021, **143**, 5445–5464.

35 N. M. Wilson, P. Priyadarshini, S. Kunz and D. W. Flaherty, *J. Catal.*, 2018, **357**, 163–175.

36 S. Kanungo, L. van Haandel, E. J. M. Hensen, J. C. Schouten and M. F. Neira d'Angelo, *J. Catal.*, 2019, **370**, 200–209.

37 J. Li, T. Ishihara and K. Yoshizawa, *J. Phys. Chem. C*, 2011, **115**, 25359–25367.

38 T. Richards, J. H. Harrhy, R. J. Lewis, A. G. R. Howe, G. M. Suldecki, A. Folli, D. J. Morgan, T. E. Davies, E. J. Loveridge, D. A. Crole, J. K. Edwards, P. Gaskin, C. J. Kiely, Q. He, D. M. Murphy, J.-Y. Maillard, S. J. Freakley and G. J. Hutchings, *Nat. Catal.*, 2021, **4**, 575–585.

39 R. J. Lewis, K. Ueura, X. Liu, Y. Fukuta, T. Qin, T. E. Davies, D. J. Morgan, A. Stenner, J. Singleton, J. K. Edwards, S. J. Freakley, C. J. Kiely, L. Chen, Y. Yamamoto and G. J. Hutchings, *ACS Catal.*, 2023, **13**, 1934–1945.

40 A. Santos, R. J. Lewis, G. Malta, A. G. R. Howe, D. J. Morgan, E. Hampton, P. Gaskin and G. J. Hutchings, *Ind. Eng. Chem. Res.*, 2019, **58**, 12623–12631.

41 J. K. Edwards, A. Thomas, A. F. Carley, A. A. Herzing, C. J. Kiely and G. J. Hutchings, *Green Chem.*, 2008, **10**, 388–394.

42 S. Stoll and A. Schweiger, *J. Magn. Reson.*, 2006, **178**, 42–55.

43 E. N. Ntainjua, J. K. Edwards, A. F. Carley, J. A. Lopez-Sanchez, J. A. Moulijn, A. A. Herzing, C. J. Kiley and G. J. Hutchings, *Green Chem.*, 2008, **10**, 1162–1169.

44 T. Richards, R. J. Lewis, D. J. Morgan and G. J. Hutchings, *Catal. Lett.*, 2022, **153**, 32–40.

45 G. Sharp, R. J. Lewis, J. Liu, G. Magri, D. J. Morgan, T. E. Davies, Á. López-Martín, R. Li, C. R. Morris, D. M. Murphy, A. Folli, A. I. Dugulan, L. Chen, X. Liu and G. J. Hutchings, *ACS Catal.*, 2024, **14**, 15279–15293.

46 F. Ni, R. J. Lewis, Á. López-Martín, L. R. Smith, D. J. Morgan, T. E. Davies, S. H. Taylor and G. J. Hutchings, *Catal. Today*, 2024, **442**, 114910.

47 R. J. Lewis, K. Ueura, X. Liu, Y. Fukuta, T. E. Davies, D. J. Morgan, L. Chen, J. Qi, J. Singleton, J. K. Edwards, S. J. Freakley, C. J. Kiely, Y. Yamamoto and G. J. Hutchings, *Science*, 2022, **376**, 615–620.

48 H. Xu, D. Cheng and Y. Gao, *ACS Catal.*, 2017, **7**, 2164–2170.

49 F. Menegazzo, M. Manzoli, M. Signoretto, F. Pinna and G. Strukul, *Catal. Today*, 2015, **248**, 18–27.

50 J. Pritchard, L. Kesavan, M. Piccinini, Q. He, R. Tiruvalam, N. Dimitratos, J. A. Lopez-Sanchez, A. F. Carley, J. K. Edwards, C. J. Kiely and G. J. Hutchings, *Langmuir*, 2010, **26**, 16568–16577.

51 A. Savara, C. E. Chan-Thaw, J. E. Sutton, D. Wang, L. Prati and V. Alberto, *ChemCatChem*, 2017, **9**, 253–257.

52 Y. Chen, H. Lim, Q. Tang, Y. Gao, T. Sun, Q. Yan and Y. Yang, *Appl. Catal., A*, 2010, **380**, 55–65.

53 J. Long, H. Liu, S. Wu, S. Liao and Y. Li, *ACS Catal.*, 2013, **3**, 647–654.

54 P. Tian, L. Ouyang, X. Xu, C. Ao, X. Xu, R. Si, X. Shen, M. Lin, J. Xu and Y. F. Han, *J. Catal.*, 2017, **349**, 30–40.

55 J. Luo, H. Yu, H. Wang, H. Wang and F. Peng, *Chem. Eng. J.*, 2014, **240**, 434–442.

56 A. Constantinou, G. Wu, B. Venezia, P. Ellis, S. Kuhn and A. Gavriilidis, *Top. Catal.*, 2019, **62**, 1126–1131.

57 C. Keresszegi, D. Ferri, T. Mallat and A. Baiker, *J. Phys. Chem. B*, 2005, **109**, 958–967.

58 W. Partenheimer, *Adv. Synth. Catal.*, 2006, **348**, 559–568.

59 M. H. Ab Rahim, M. M. Forde, R. L. Jenkins, C. Hammond, Q. He, N. Dimitratos, J. A. Lopez-Sanchez, A. F. Carley, S. H. Taylor, D. J. Willock, D. M. Murphy, C. J. Kiely and G. J. Hutchings, *Angew. Chem., Int. Ed.*, 2013, **52**, 1280–1284.

60 A. Santos, R. J. Lewis, D. J. Morgan, T. E. Davies, E. Hampton, P. Gaskin and G. J. Hutchings, *Catal. Sci. Technol.*, 2021, **11**, 7866–7874.

61 J. Marugán, D. Hufschmidt, M.-J. López-Muñoz, V. Selzer and D. Bahnemann, *Appl. Catal., B*, 2006, **62**, 201–207.

62 M. R. Billany, K. Khatib, M. Gordon and J. K. Sugden, *Int. J. Pharm.*, 1996, **137**, 143–147.

63 G. R. Buettner, *Free Radical Biol. Med.*, 1987, **3**, 259–303.

64 J. Zhang, S. Xiao, R. Chen and F. Chen, *J. Chem. Technol. Biotechnol.*, 2019, **94**, 1613–1621.

65 Y. Zhao, C. Yu, S. Wu, W. Zhang, W. Xue and Z. Zeng, *Catal. Lett.*, 2018, **148**, 3082–3092.

66 N. M. Wilson and D. W. Flaherty, *J. Am. Chem. Soc.*, 2016, **138**, 574–586.